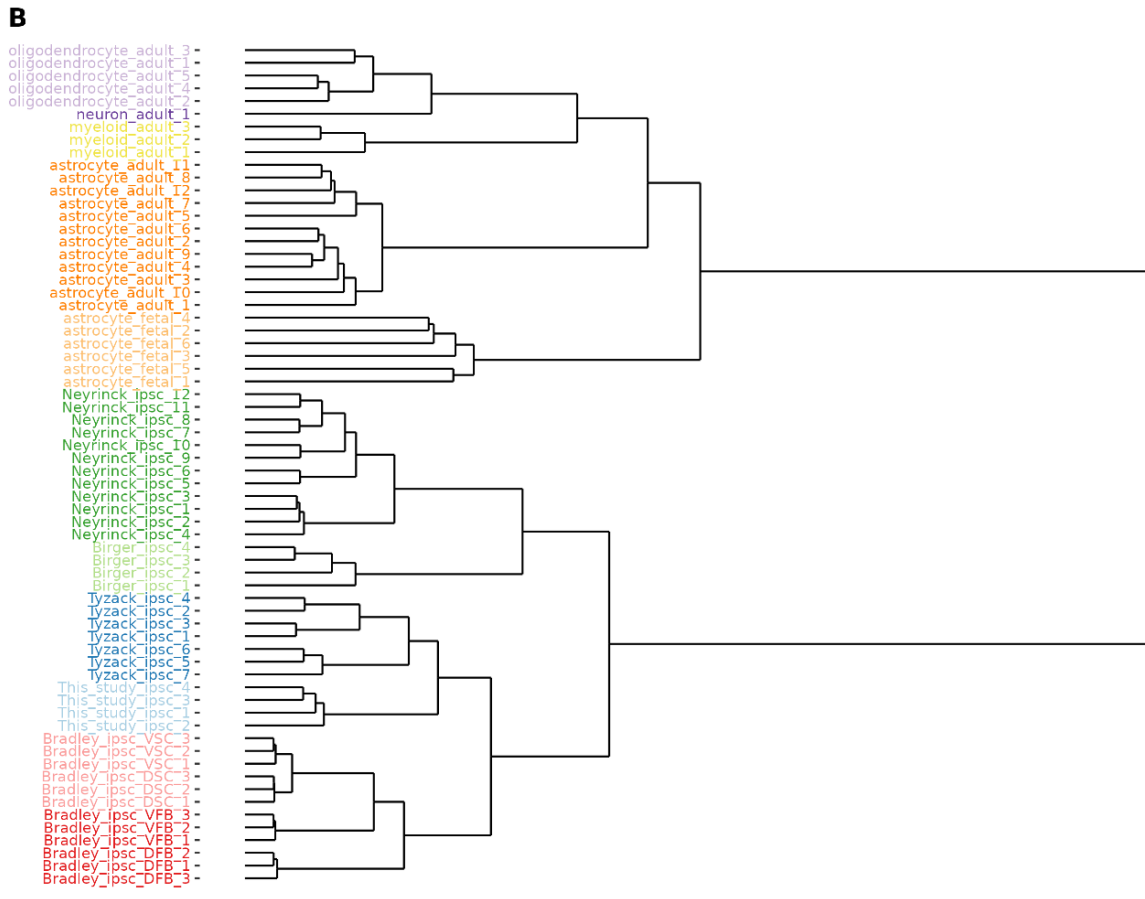
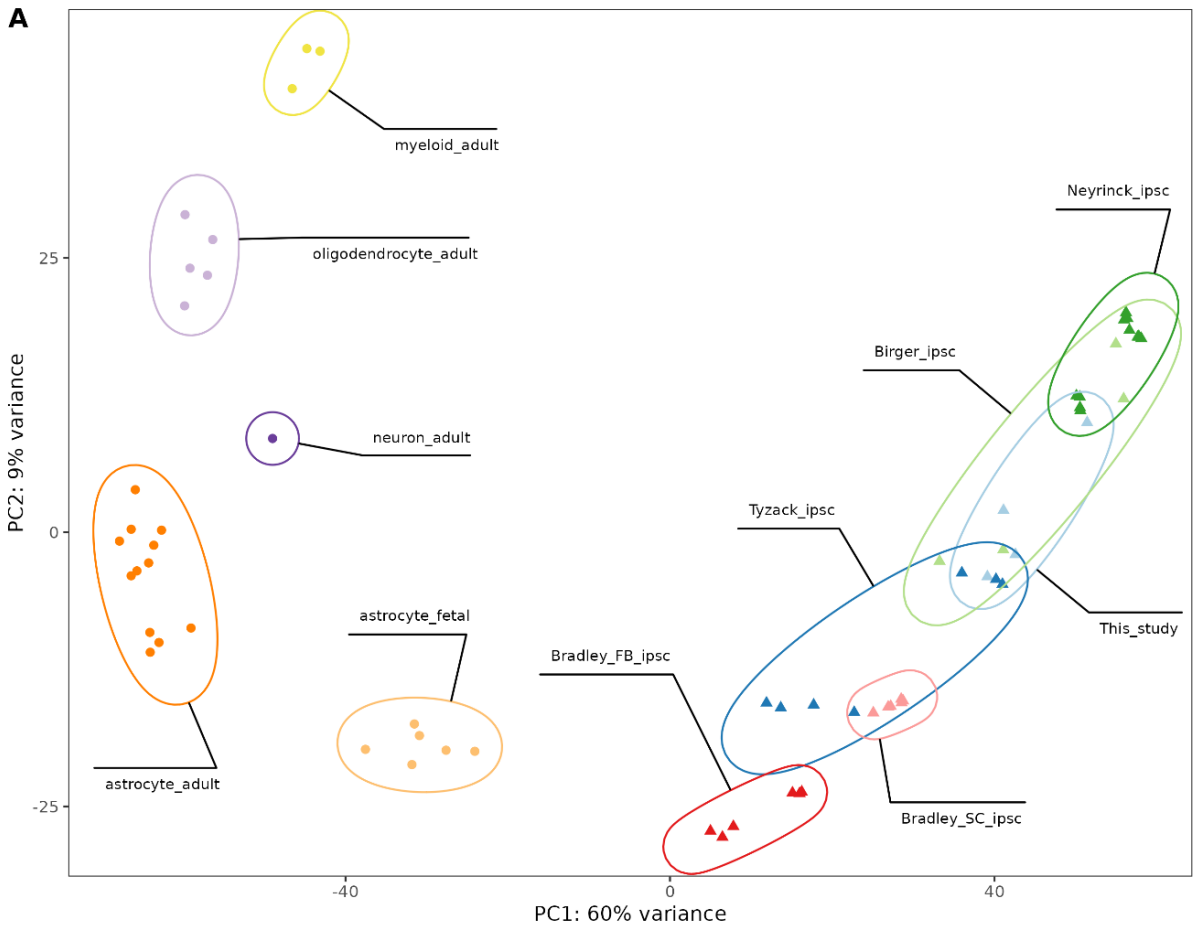


SUPPLEMENTAL FIGURES

Meta-analysis of human and mouse ALS astrocytes reveals multiomic signatures of inflammatory reactive states

Oliver J. Ziff^{1,2,3}#, Benjamin E. Clarke^{1,2}#, Doaa M. Taha^{1,2,4}#, Hamish Crerar^{1,2},

Nicholas M. Luscombe^{1,5,6}, Rickie Patani^{1,2,3}*

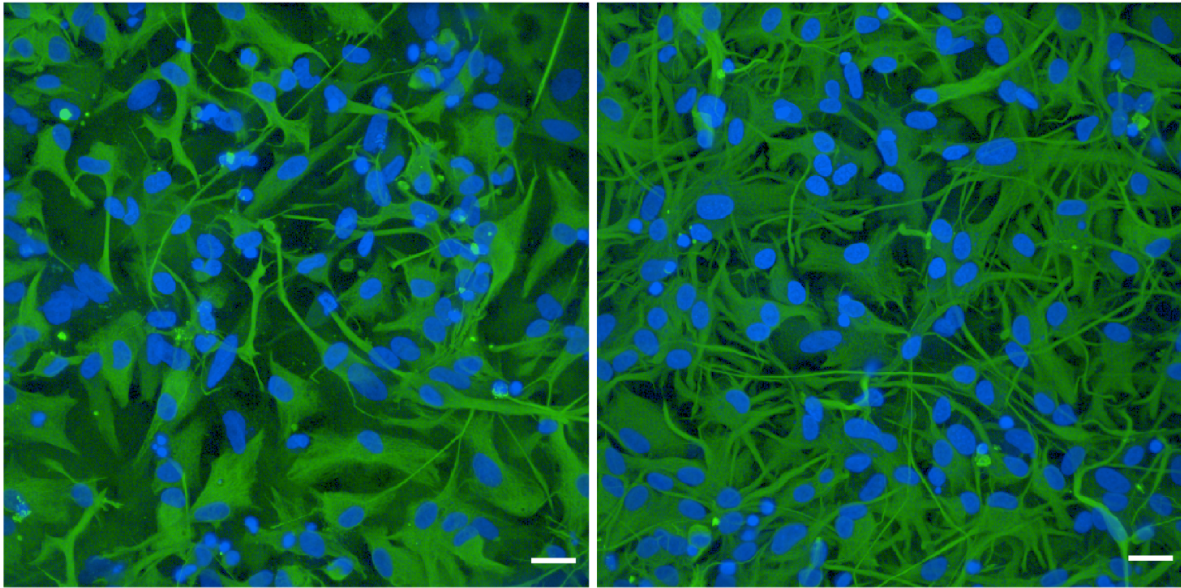


Supplementary Figure 1

A: Principal component analysis (PCA) on variance stabilised gene counts plotted by their coordinates along the first two principal components across all human samples. Samples include human biopsy purified cell type samples from Zhang et al. 2016 (Neuron, Myeloid, Oligodendrocyte, adult and fetal Astrocyte) together with hiPSC-astrocytes (This study: *VCP* mutant and control, Tyzack: *SOD1* mutant and control, Birger: *C9orf72* mutant and control, Neyrinck: *FUS* mutant and control and Bradley: regionally specified dorsal (D) and ventral (V) forebrain (FB) and dorsal and ventral spinal cord (SC). Samples are labeled and coloured by their dataset and shape according to source tissue.

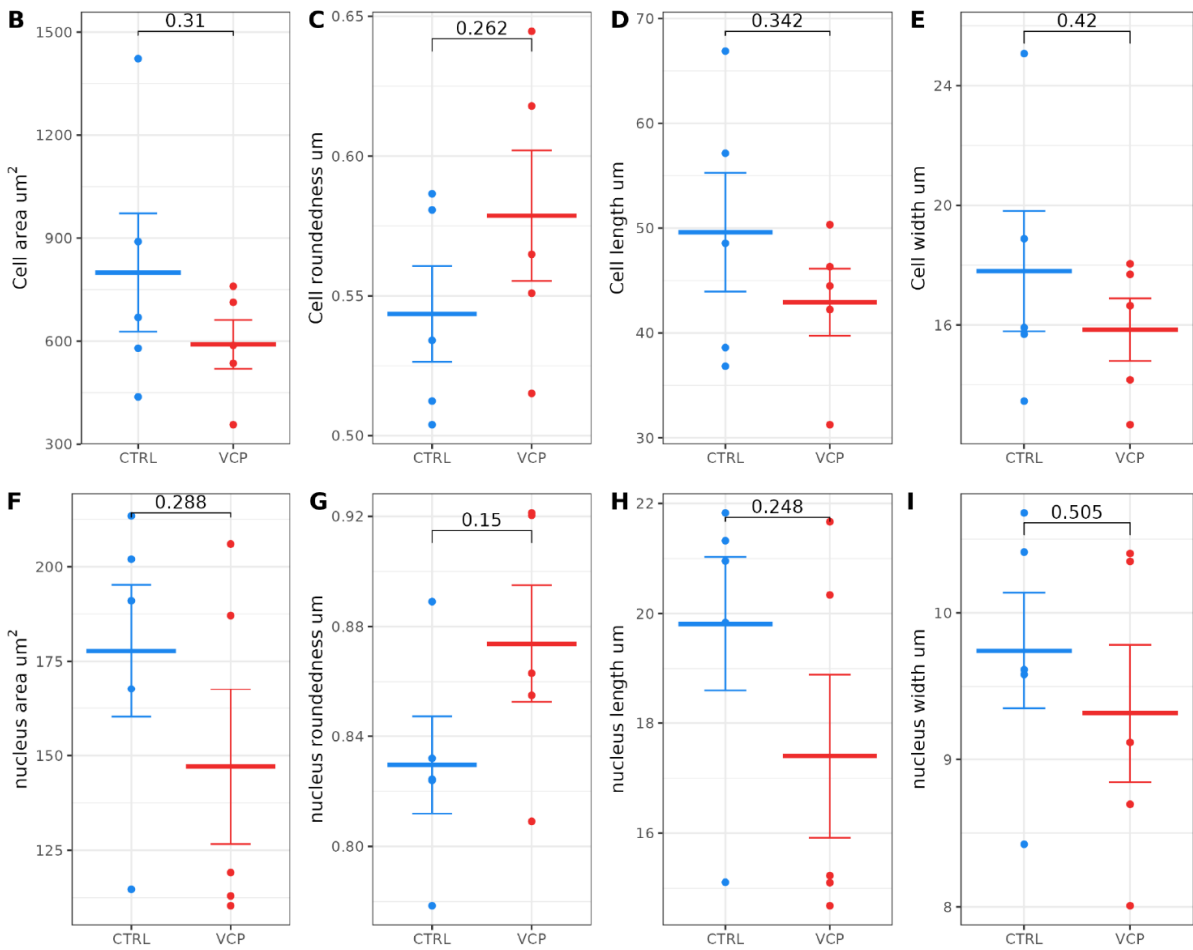
B: Dendrogram showing unsupervised hierarchical clustering of variance stabilised gene counts across the same samples.

A GFAP/DAPI



CTRL

VCP mutant

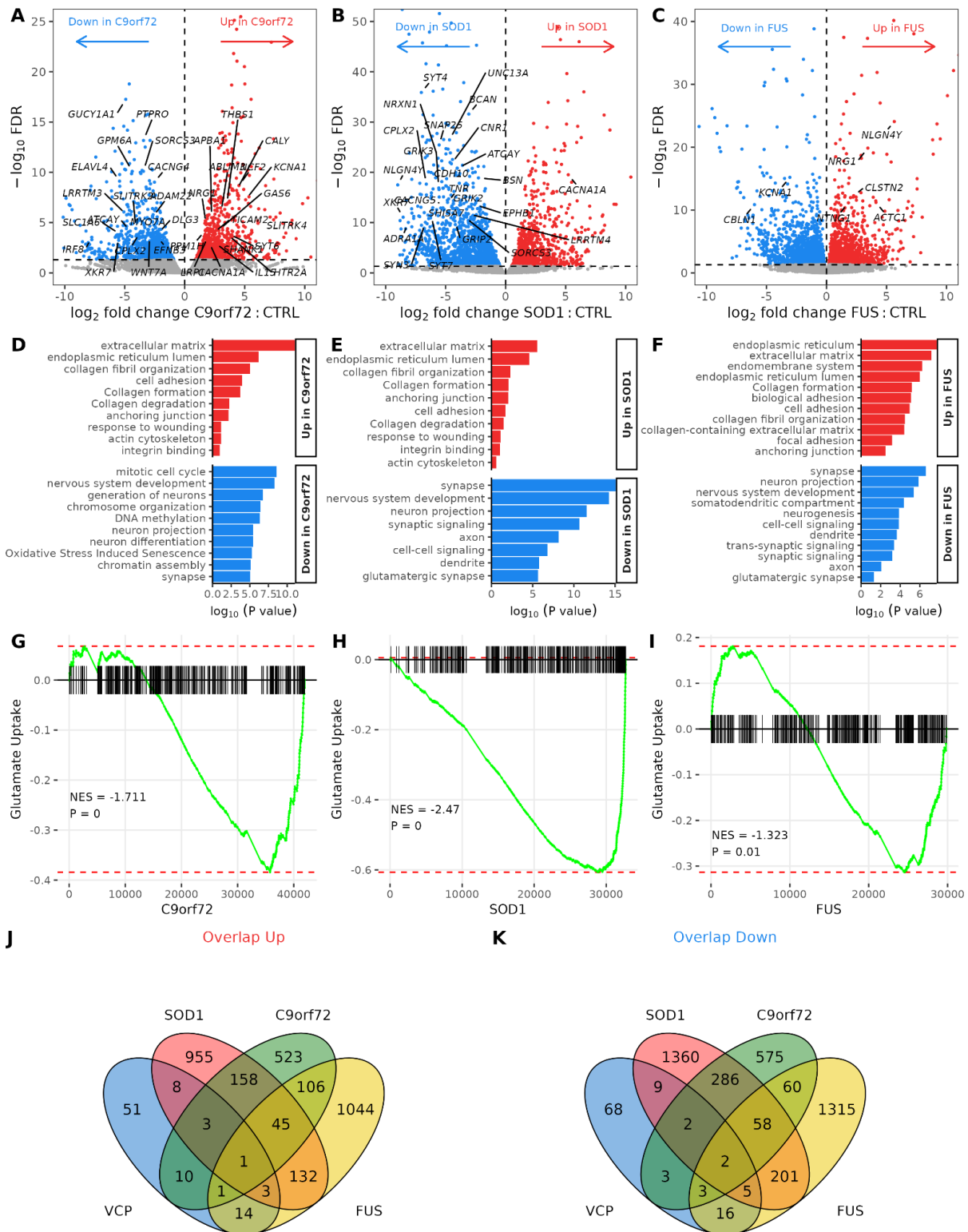


Supplementary Figure 2

A: Representative immunolabeling images of control (left) and *VCP* mutant (right) astrocytes staining for GFAP (green). Nuclei were counterstained by DAPI (blue). Scale bar, 20um.

B-E: Quantification of morphological parameters of whole cell astrocytes in controls (blue, n = 5) and *VCP* mutants (red, n=5).

F-I: Quantification of morphological parameters of astrocyte nucleus in controls (blue, n = 5) and *VCP* mutants (red, n = 5). Results plotted are the mean of 2 technical repeats from 2 experimental repeats. 2-3 biological lines were used in both control and *VCP* mutant for each experimental repeat. P values are reported from the t-test.



Supplementary Figure 3

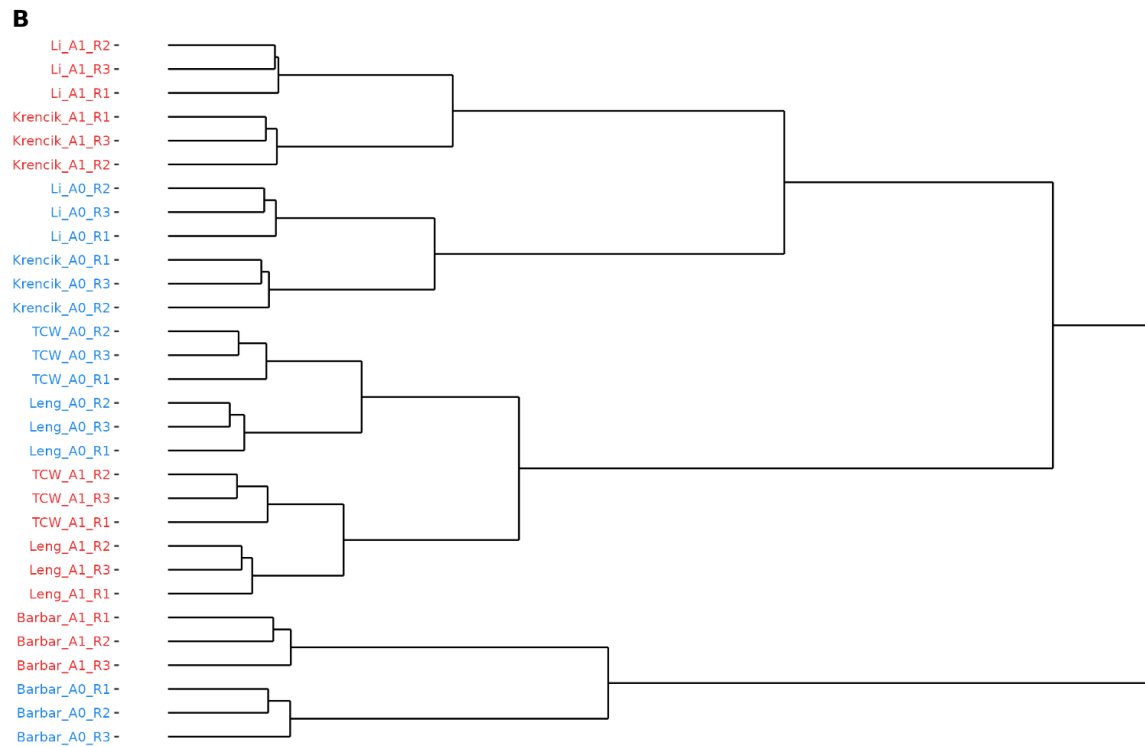
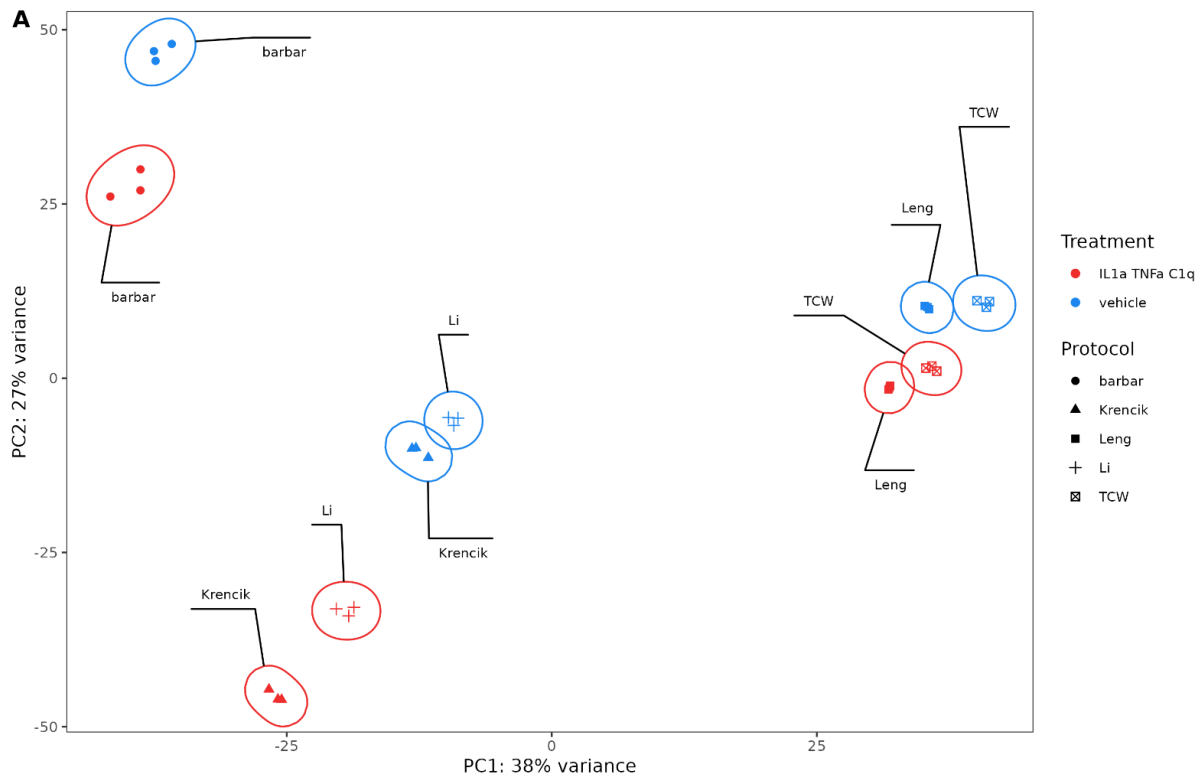
A-C: Volcano plots showing \log_2 fold change in differential gene expression from RNA sequencing for ALS mutant *C9orf72* (A), *SOD1* (B) and *FUS* (C) versus control astrocytes. Genes with significantly

(FDR < 0.05) increased expression are shown in red and those decreased in expression are shown in blue.

D-F: Gene ontology terms enriched in up (red) and downregulated (blue) differentially expressed genes in ALS mutant *C9orf72* (D), *SOD1* (E) and *FUS* (F) vs control astrocytes.

G-I: Gene set enrichment analyses (GSEA) plots for glutamate uptake in *C9orf72* (G), *SOD1* (H), *FUS* (I).

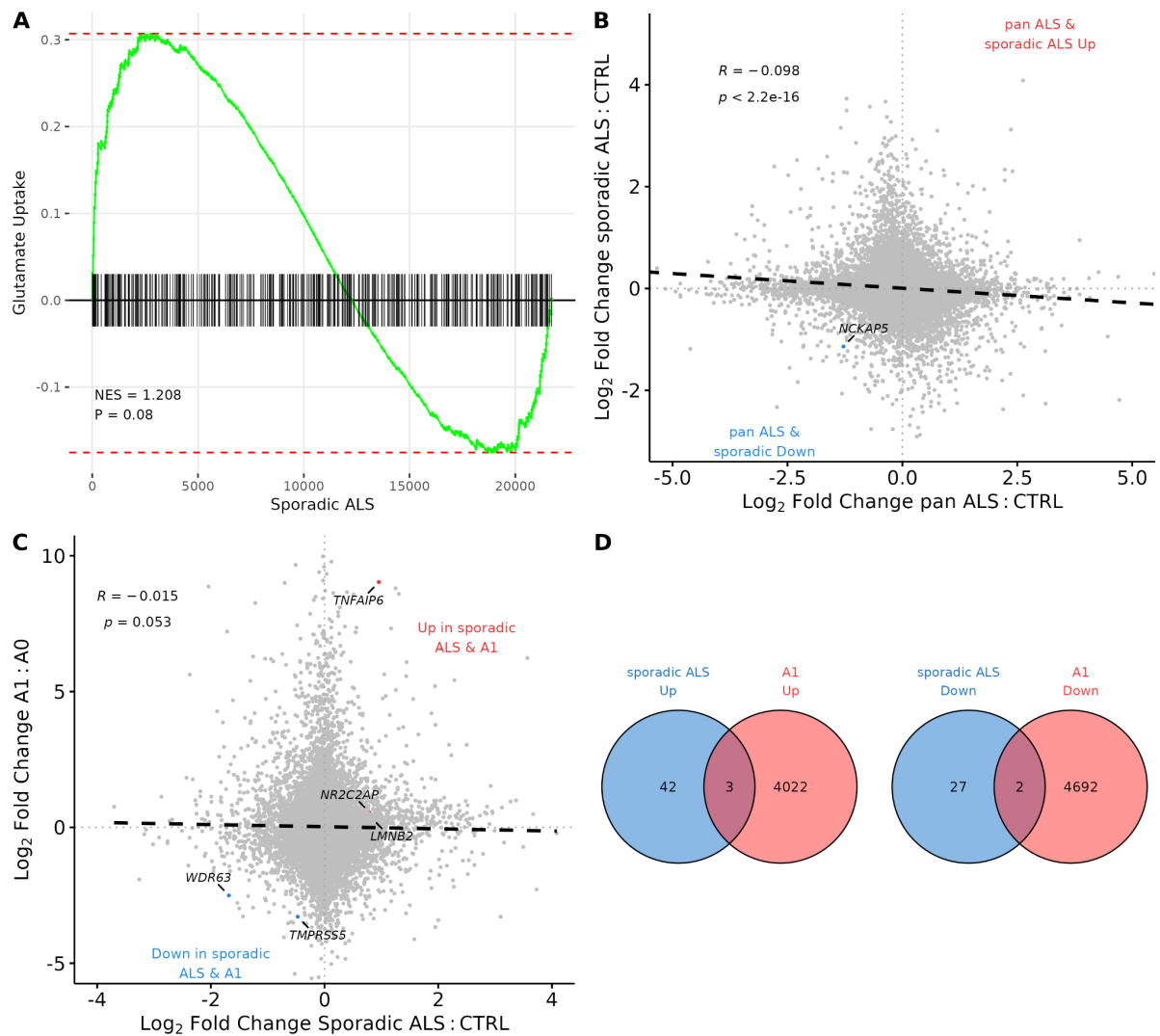
J-K: Venn diagrams showing overlapping differentially expressed genes between *VCP* (blue), *SOD1* (red), *C9orf72* (green) and *FUS* (yellow) for upregulated (J) and downregulated (K) genes. See Table S3 for details of overlapping genes.



Supplementary Figure 4

A: Principal component analysis (PCA) on variance stabilised gene counts plotted by their coordinates along the first two principal components across TNF, IL1A, C1q and vehicle treated hiPSC derived astrocyte samples.

B: Dendrogram showing unsupervised hierarchical clustering of variance stabilised gene counts across the same samples.



Supplementary Figure 5

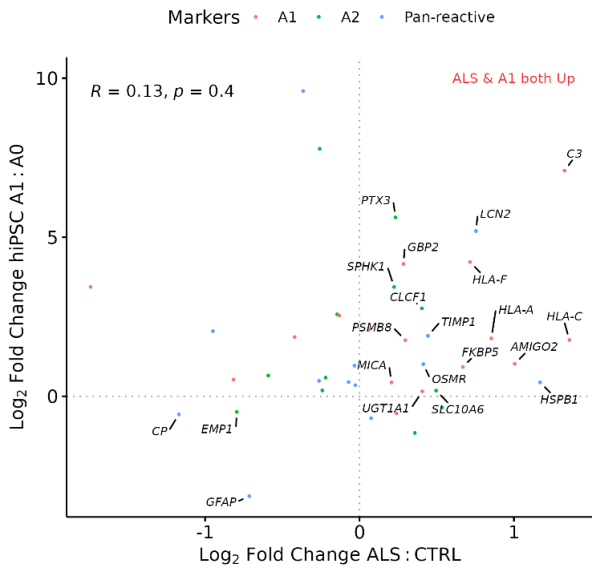
A: Gene set enrichment analysis of glutamate uptake in sporadic ALS astrocytes

B: Scatterplot of meta-analysis panALS vs control (x-axis) against log₂ fold change in sporadic ALS vs control microarray.

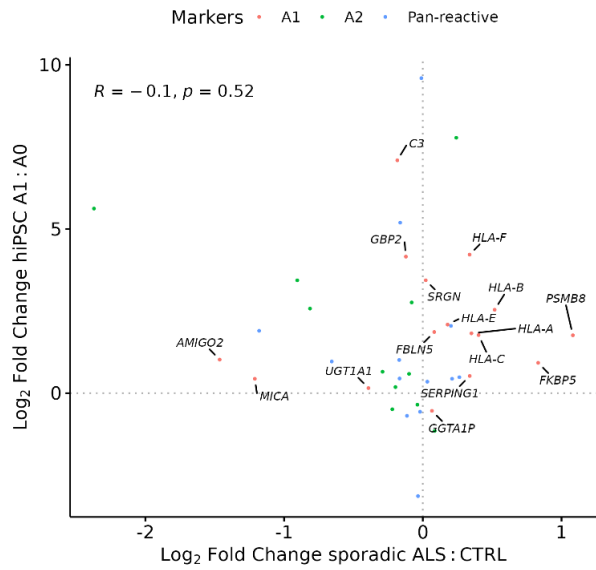
C: Scatterplot of sporadic ALS vs control (x-axis) against log₂ fold change in hiPSC A1 vs A0

D: Venn overlap of differentially expressed genes in sporadic ALS (blue) and A1 (red) hiPSC astrocytes.

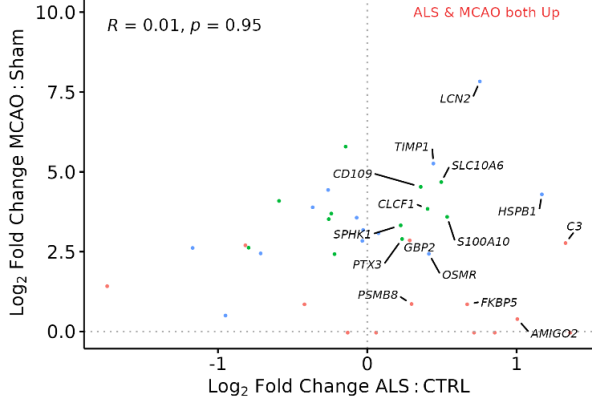
A hiPSC A1 and ALS astrocytes : Liddelow markers



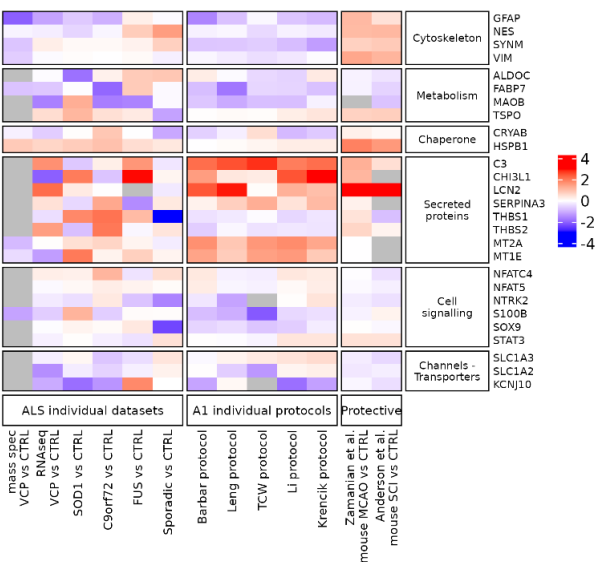
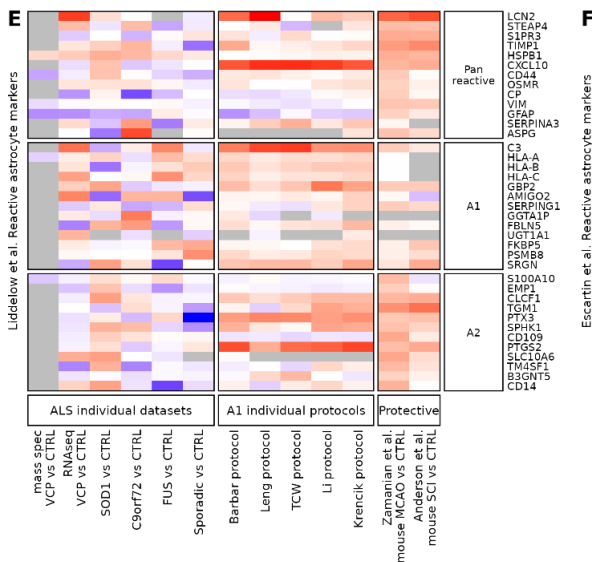
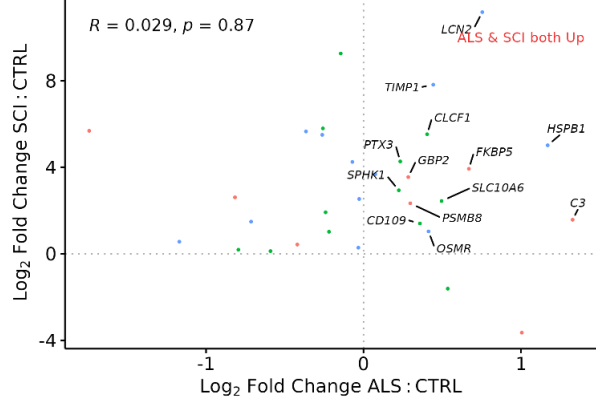
B hiPSC A1 and sporadic ALS astrocytes : Liddelow markers



C MCAO and ALS astrocytes : Liddelow markers



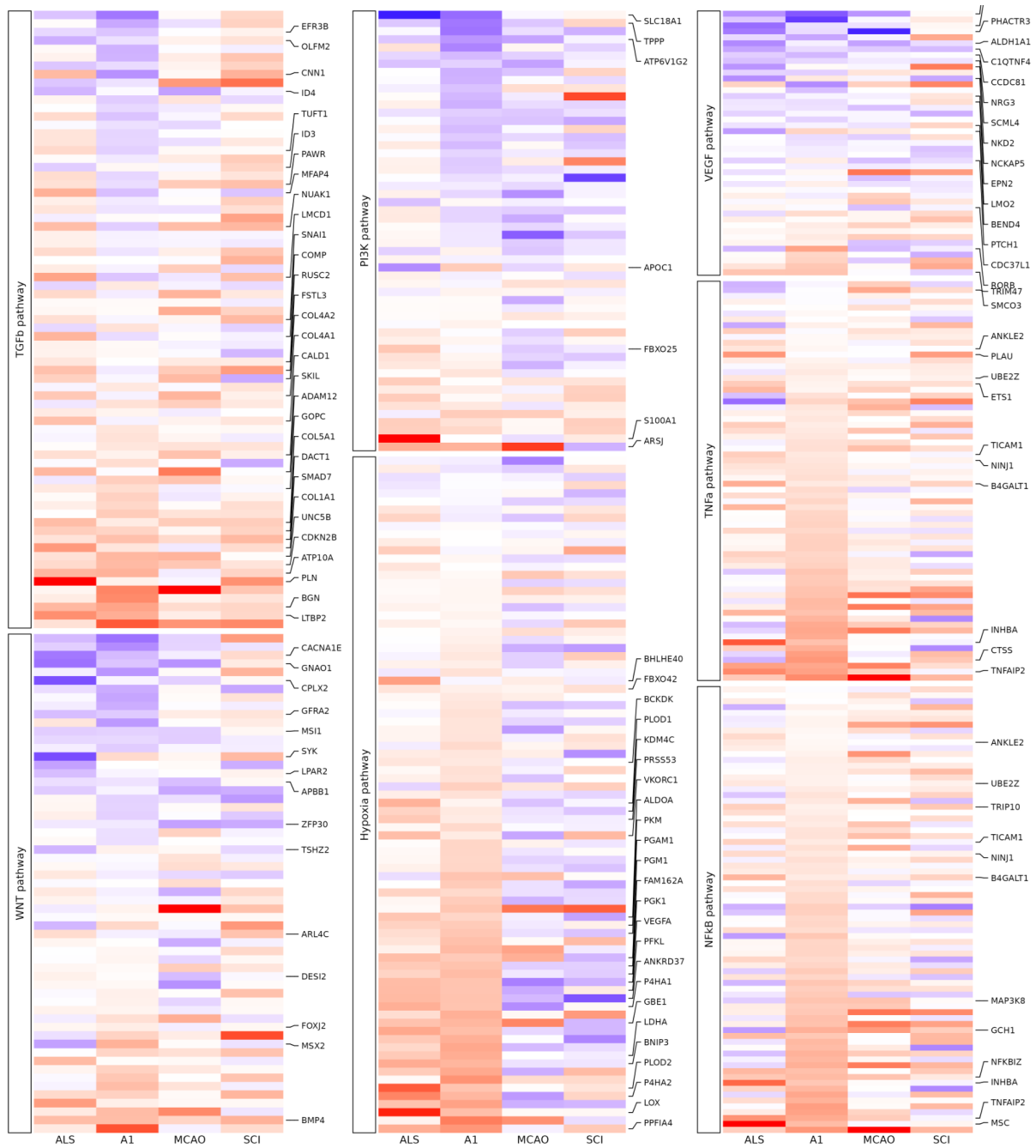
D SCI and ALS astrocytes : Liddelow markers



Supplementary Figure 6

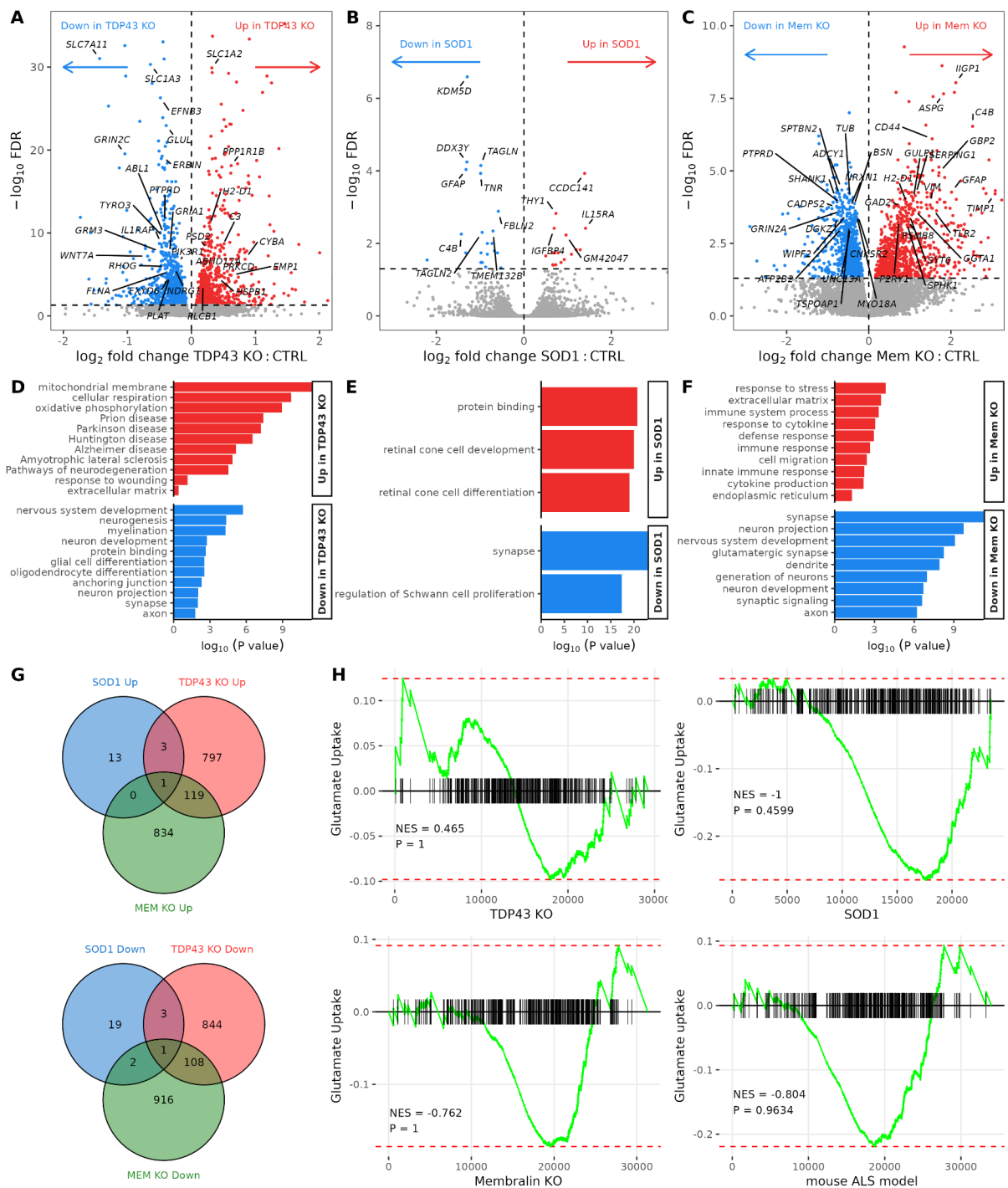
A-D: Scatterplots of (Liddelow et al. 2017) astrocyte reactivity markers showing \log_2 fold change in hiPSC A1 vs A0 (y-axis) against (A) pan ALS vs control, (B) sporadic ALS vs control (x-axis) and pan ALS vs control (x-axis) against in (C) MCAO vs Sham, (D) SCI vs control (y-axis).

E-F: Heatmaps of (Liddelow et al. 2017) pan-reactive, A1 and A2 specific astrocyte reactivity markers (E) and (Escartin et al. 2021) markers of astrocyte reactivity (F; rows) in the hiPSC ALS astrocyte individual datasets, hiPSC A1 protocols (TNF, IL1A, C1q vs vehicle) and protective astrocyte datasets (columns). Colour intensity represents the scaled differential gene expression \log_2 fold changes in each dataset.



Supplementary Figure 7

PROGENy signaling pathway responsive genes for the top 6 pathways upregulated in pan-ALS vs control. Each heatmap shows the log₂ fold change in (left to right columns) pan-ALS vs control, hiPSC A1 vs A0, MCAO vs sham, SCI vs control. Genes changing significantly in ALS (FDR < 0.05) are labelled.



Supplementary Figure 8

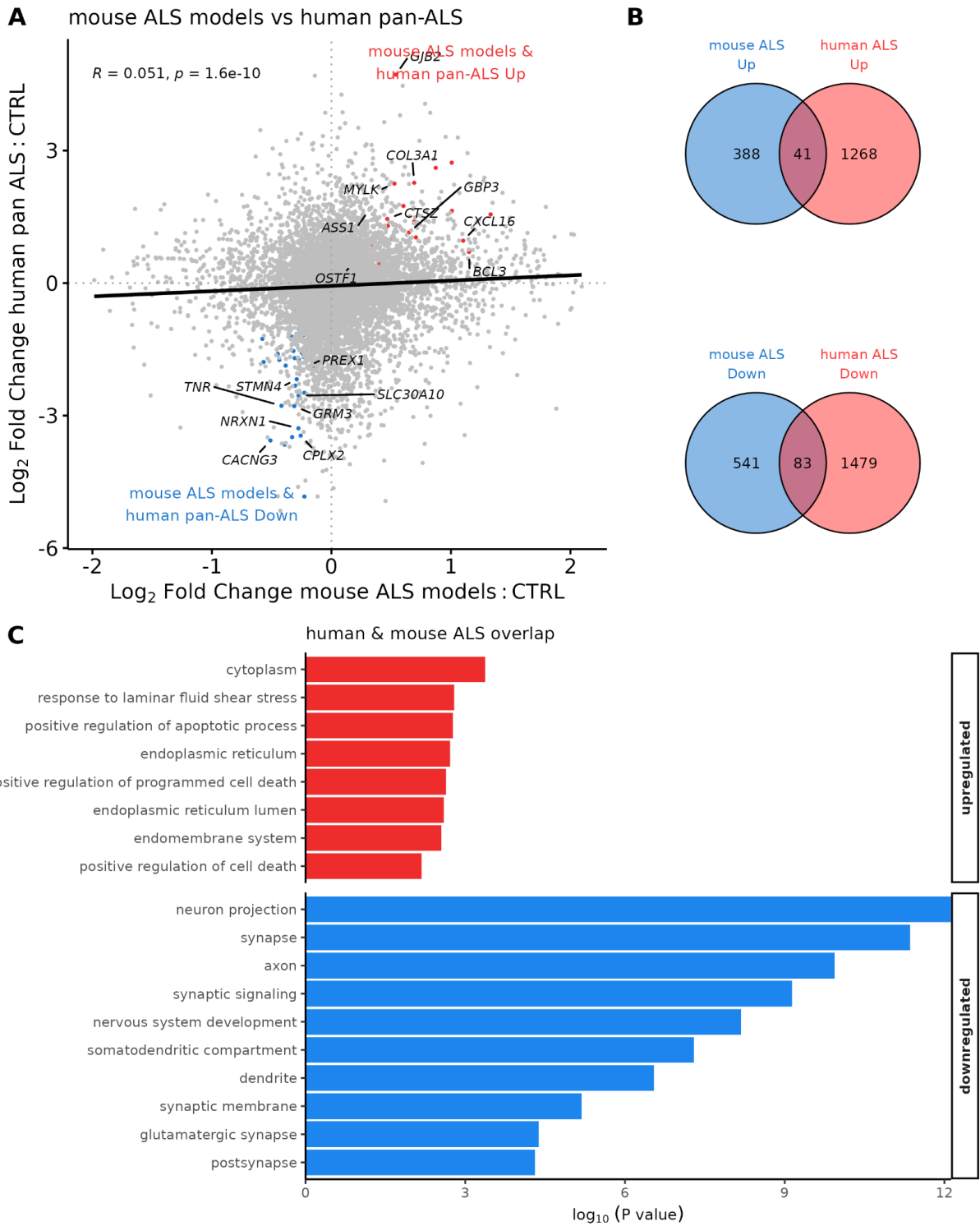
A-C: Volcano plots showing \log_2 fold change in differential gene expression from RNA sequencing for ALS mutant (A) Tardbp knockout, (B) Sod1^{G93A} and (C) membralin knockout versus control mouse astrocytes. Genes with significantly (FDR < 0.05) increased expression are shown in red and those

decreased in expression are shown in blue.

D-F: Gene ontology terms enriched in up (red) and downregulated (blue) differentially expressed genes in ALS mutant (D) Tardbp knockout , (E) Sod1^{G93A} and (F) membralin knockout vs control astrocytes.

G: Venn diagrams showing overlapping differentially expressed genes between Sod1^{G93A} (blue), Tardbp knockout (red), membralin knockout (green) for upregulated (top) and downregulated (bottom) genes.

H: Gene set enrichment analyses (GSEA) plots for glutamate uptake in Tardbp KO (top left), Sod1^{G93A} (top right), membralin KO (bottom left) and mouse ALS meta-analysis (bottom right).

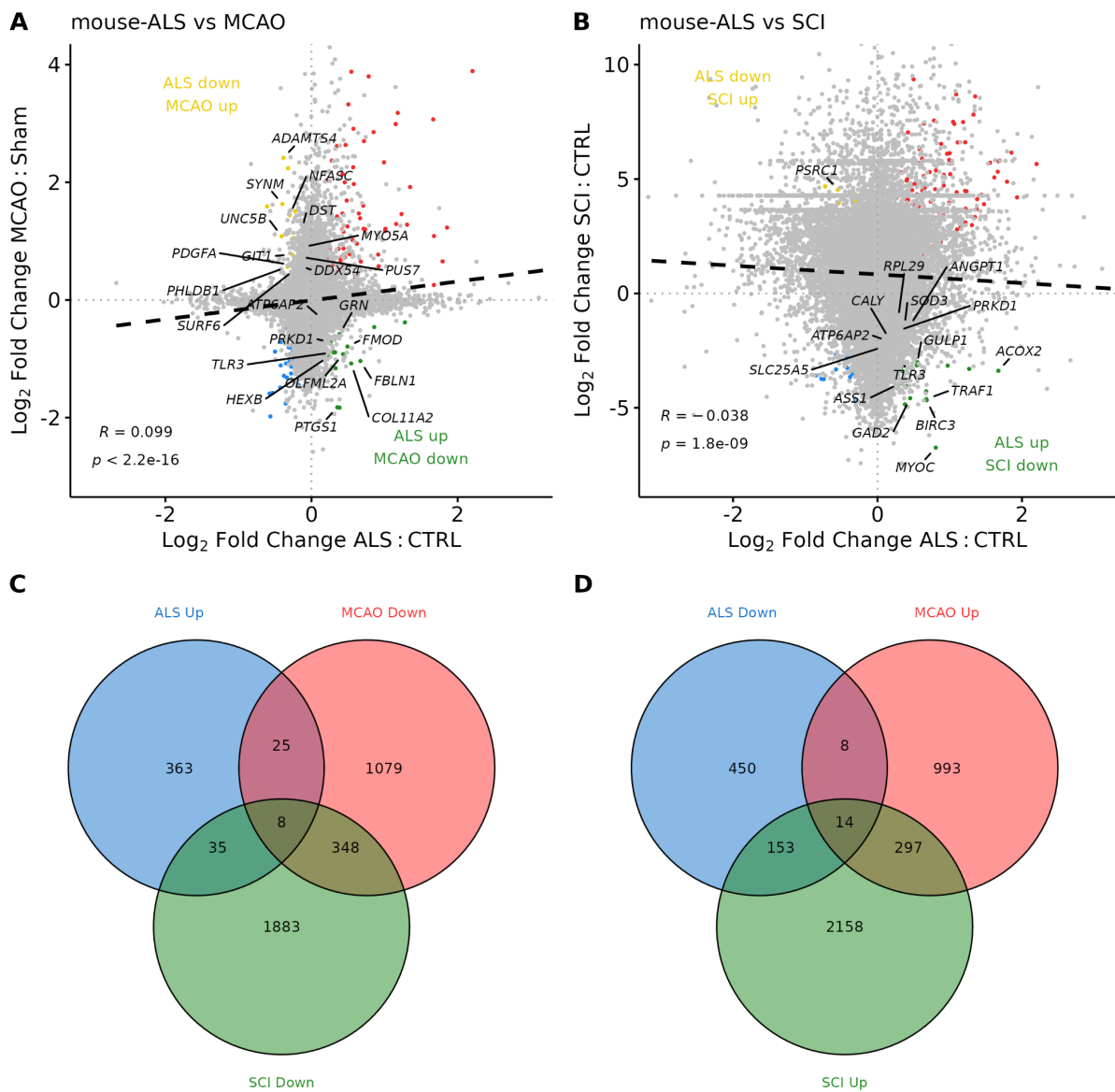


Supplementary Figure 9

A: Scatterplot of human and mouse meta-analyses: log₂ fold change in human ALS vs control (y-axis) against log₂ fold change in mouse ALS models vs control (y-axis). Genes coloured red are upregulated in both meta-analyses whilst blue genes are downregulated in both.

B: Venn overlap of differentially expressed genes in the human ALS meta-analysis (red) and mouse ALS models meta-analysis (blue) for upregulated (top) and downregulated (bottom) genes.

C: Bar graph showing curated overrepresented functional categories (FDR < 0.05) by gene ontology analysis of genes co-upregulated (red) and co-downregulated (blue) between human pan-ALS and mouse ALS model meta-analyses.

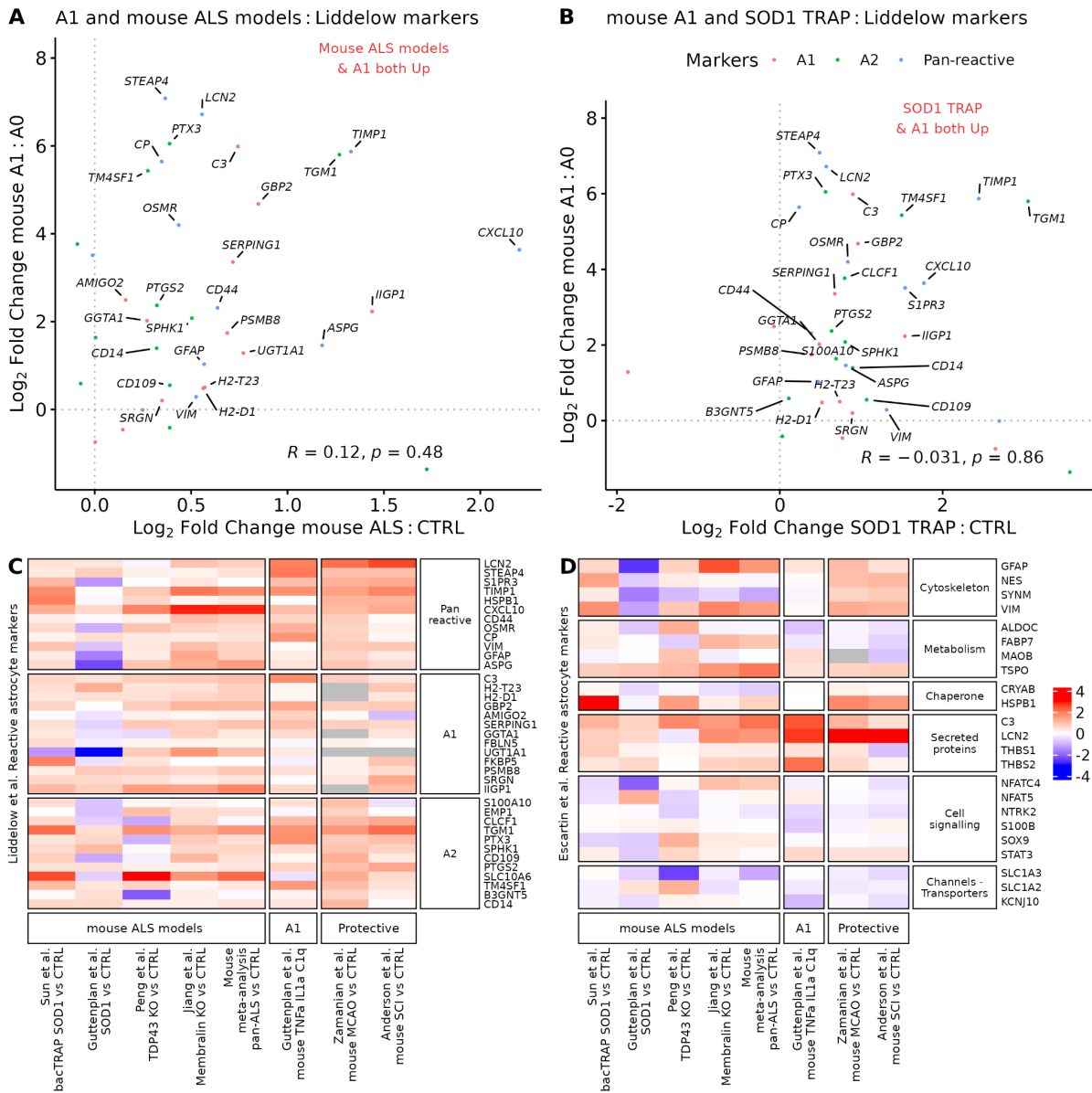


Supplementary Figure 10

A-B: Scatterplots of log₂ fold changes in gene expression in mouse ALS vs control astrocytes (x-axis) against (A) MCAO vs Sham astrocytes and (B) SCI vs control astrocytes (y-axis). Black dashed line indicates linear regression correlation (Pearson correlation MCAO $R = +0.1$, SCI $R = -0.04$). Overlapping differentially expressed genes are coloured red (upregulated) and blue (downregulated). Genes increased in ALS but decreased in the protective astrocytes are shown in green, whilst genes decreased in ALS and increased in protective astrocytes are yellow.

C-D: Venn diagram depicting the number of differentially expressed genes (FDR < 0.05) increased

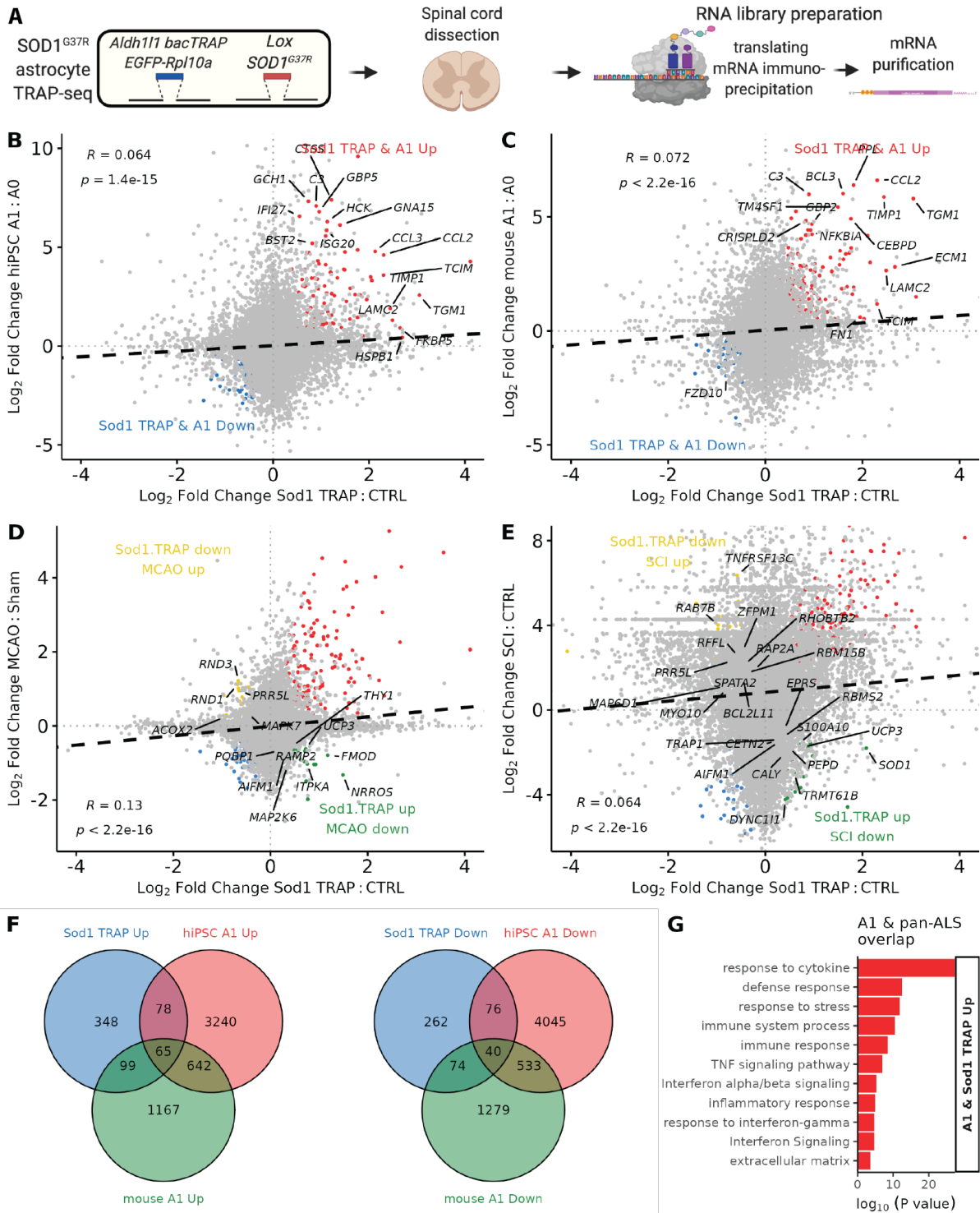
(up) in ALS but decreased (down) in the protective astrocytes (C) and genes decreased in ALS but increased in protective astrocytes (D).



Supplementary Figure 11

A-B: Scatterplots of (Liddelow et al. 2017) astrocyte reactivity markers showing log₂ fold change in (A) mouse ALS models vs control and (B) Sod1 TRAP mouse vs control (x-axis) against log₂ fold change in mouse A1 vs A0 (y-axis).

C-D: Heatmaps of (Liddelow et al. 2017) pan-reactive, A1 and A2 specific astrocyte reactivity markers (C) and (Escartin et al. 2021) markers of astrocyte reactivity (D; rows) in the mouse ALS models individual datasets (left columns) and meta-analysis and A1 and protective datasets (columns). Colour intensity represents the scaled differential gene expression log₂ fold changes in ALS vs control; A1 vs A0 astrocytes.



Supplementary Figure 12

A: Schematic depicting mouse in vivo (top row) ALS Sod1^{G37R} mutant mouse with astrocyte-specific (Aldh1l1) bacTRAP reporter, which expresses the EGFP-tagged ribosome protein (Rpl10a) within astrocytes. Polyribosome-associated mRNAs undergoing translation are then isolated by EGFP immunoprecipitation before mRNA purification and RNA translome sequencing. B-E: Scatterplots of log₂ fold changes in gene expression in astrocyte-specific bacTRAP mouse Sod1 mutant vs control (x-axis) against log₂ fold changes in (B) hiPSC A1 vs A0 astrocytes, (C) mouse A1 vs A0 astrocytes, (D) middle cerebral artery occlusion (MCAO) vs sham, and (E) spinal cord injury (SCI) vs control (y-axis) against. Black dotted line indicates linear regression correlation (Pearson correlation R reported in each plot). Overlapping differentially expressed genes are coloured red (upregulated, top right quadrant) and blue (downregulated, bottom left quadrant).

F: Venn diagrams depicting the overlap of upregulated (left) and downregulated (right) differentially expressed genes between bacTRAP Sod1 (blue), hiPSC A1 (red) and mouse A1 (green) astrocytes.

G: Bar graph showing curated overrepresented functional categories (FDR < 0.05) by gene ontology analysis of 154 genes Sod1 TRAP, hiPSC & mouse A1 co-upregulated (red). There were no relevant terms enriched amongst the 102 co-downregulated (blue) genes.